

Investigating uplift in Lesina Marina (Southern Italy) with the aid of persistent scatterer SAR interferometry and in situ measurements

A. Refice¹ · G. Pasquariello¹ · F. Bovenga¹ · V. Festa² · P. Acquafredda² · G. Spilotro³

Received: 24 March 2015 / Accepted: 29 September 2015 / Published online: 25 January 2016
© The Author(s) 2015. This article is published with open access at Springerlink.com

Abstract We apply persistent scatterer interferometry (PSI) techniques to synthetic aperture radar (SAR) data from ERS and ENVISAT satellites on the Lesina Marina area, a coastal tourist village in Apulia, Southern Italy, where the excavation of a canal exposed grey micro- and meso-crystalline gypsum which is now showing a high density of cavities and sinkholes due to gravitational collapse processes. We observe PS objects undergoing displacements, along the sensor line of sight, forming the same relatively smooth pattern in all the processed data stacks. Vertical displacement rates, derived through integration of ascending and descending geometries, reach about 4 mm/year on locations adjacent to the canal, gently decreasing towards the western end of the built-up area. High-precision leveling measurements, performed in 1999 and 2010, reveal a substantial agreement with the

ENVISAT PSI data, taking into account a small bias due to the choice of the leveling reference point. The dataset, thus validated, suggests the presence of an uplift phenomenon going on steadily for the entire timespan covered by the SAR observations (1992–2009). These observations, supported by petrographic data and in situ investigations, seem only in part compatible with a residual diapirism, and hint instead to more complex processes, such as a combination of diapirism and the hydration of the residual anhydrite in the core of the gypsum mass. These results confirm the importance of the integration between in situ, geologic and geophysical, remotely sensed investigations, as the latter often represent an essential tool to infer whether a given phenomenon, which can be hypothesized by the former, is presently under development.

keywords Persistent scatterers SAR interferometry · Anhydrite hydration · Leveling · Petrography · Lesina marina

✉ A. Refice
refice@ba.issia.cnr.it

G. Pasquariello
pasquariello@ba.issia.cnr.it

F. Bovenga
bovenga@ba.issia.cnr.it

V. Festa
vincenzo.festa@uniba.it

P. Acquafredda
pasquale.acquafredda@uniba.it

G. Spilotro
giuseppe.spilotro@unibas.it

¹ Istituto di Studi sui Sistemi Intelligenti per l'Automazione, Consiglio Nazionale delle Ricerche (ISSIA-CNR), Bari, Italy

² Dip. di Scienze della Terra e Geoambientali, Università degli Studi di Bari "Aldo Moro", Bari, Italy

³ DICEM, Università della Basilicata, Matera, Italy

Introduction

The village of Lesina Marina is sited between the Lesina Lagoon and the mouth of the Fortore River, on the coastal plain that extends along the northern Apulia Adriatic coastline (southern Italy, see Fig. 1a). Standing only a few meters above the sea level, the village is a renowned tourist leisure area. It lies not far from the Pietre Nere (Black Stones) Point, a very interesting site and the only outcrop of magmatic rocks in the Apulia region and in the whole Adriatic coast of Italy.

In the area, an exotic rock body basically composed of Triassic gypsum crops out on a very gentle ridge, on its sides surrounded and covered by relatively thin Quaternary

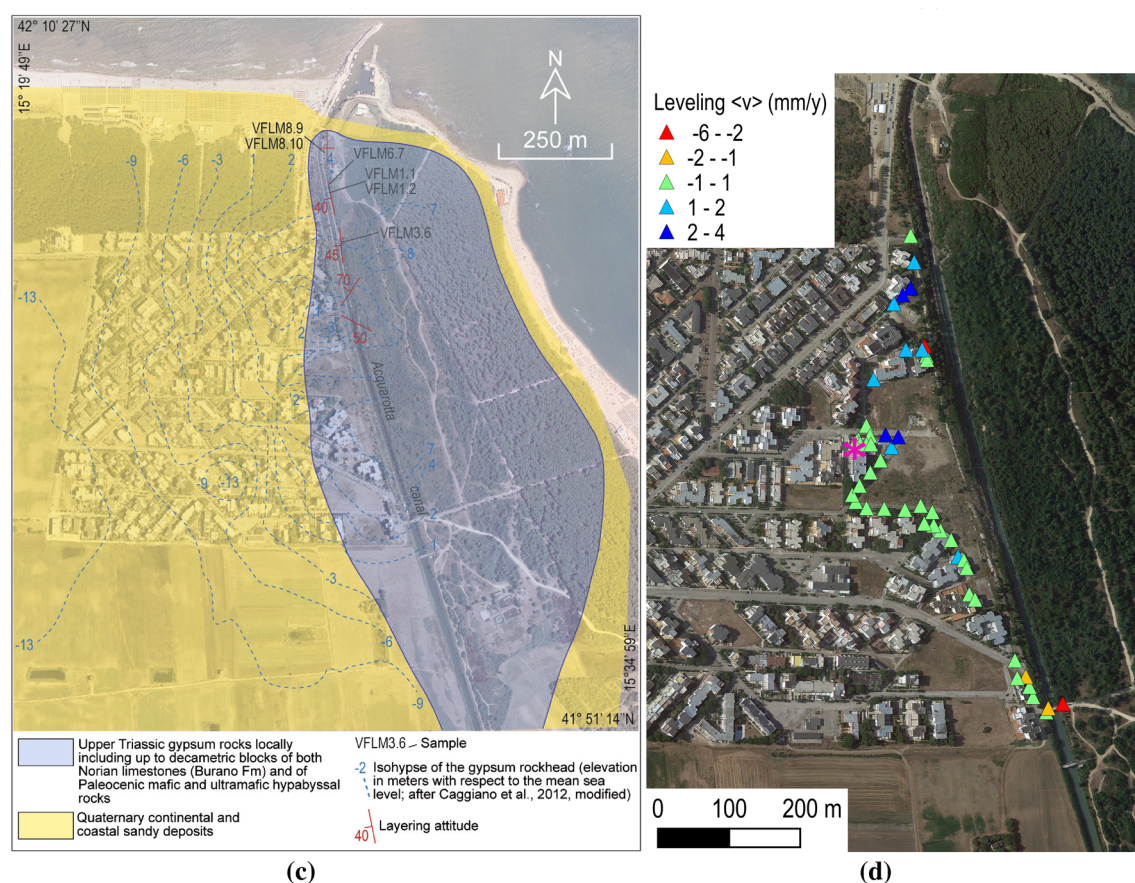
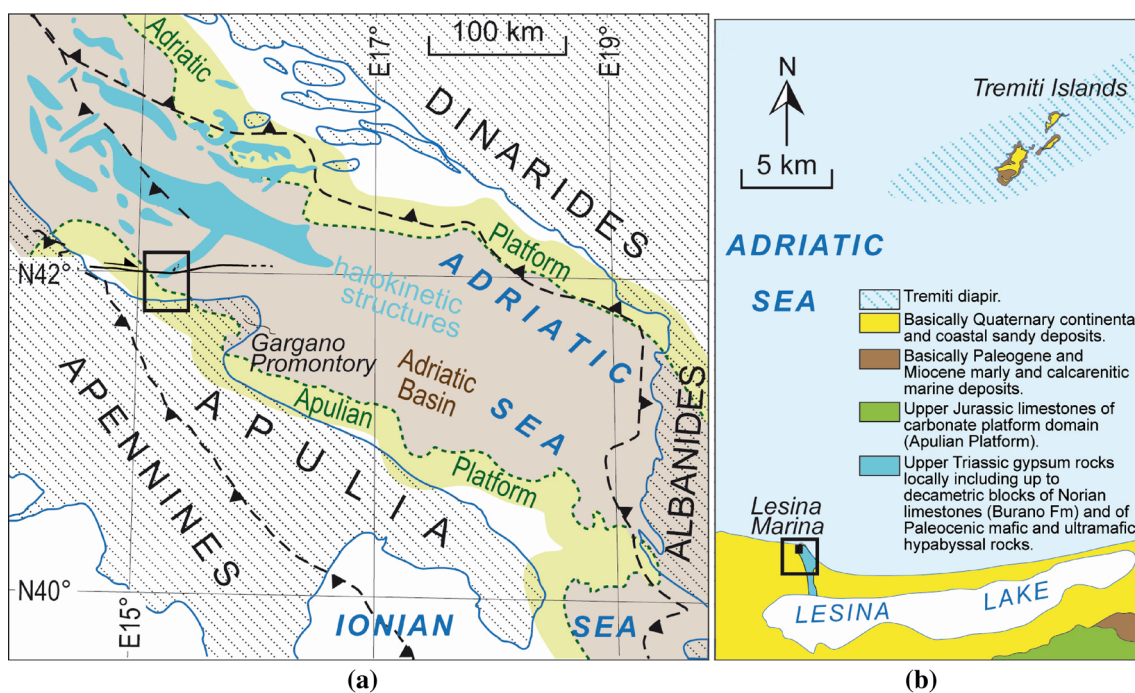


Fig. 1 **a** Schematic structural map of the Periadriatic region around the Adriatic Sea (modified from Zappaterra 1990, 1994). The Mesozoic paleogeographic position of the Adriatic Basin between the Apulian and Adriatic carbonate platforms is shown. The fronts of Apennines and Dinarides according to Scrocca (2006) and Fantoni and Franciosi (2010), respectively. The halokinetic structures are also indicated (modified from Geletti et al. 2008). **b** Schematic geological map of northern Apulia, around the area of Lesina Marina village and of the Tremiti Islands (modified from Boni et al. 1969; Cremonini et al. 1971) the location of the underlying halokinetic structure called Tremiti diapir is also indicated (modified from Festa et al. 2014). **c** Schematic geological map of the Lesina Marina village area. **d** Leveling measurements map

sandy deposits (e.g. Carella 1963) (Fig. 1b). The area of Lesina Marina is characterized by a tectonic uplift since Middle Pleistocene (Ciaranfi et al. 1983). An average uplift rate of ca. 1.5 mm/year was calculated by Mastronuzzi and Sansò (2002) for the Holocene.

The excavation of a canal through this area, performed in 1930, exposed grey micro- and meso-crystalline gypsum with intercalations of black limestones and marls of Upper Triassic age, mantled by loose sandy Quaternary deposits. Besides their uniqueness in the surface geology of southern Italy (e.g. Martinis and Pieri 1964), the importance of these gypsum rocks is also related to the large number of cavities, either dissolutional conduits or voids related to gravitational collapse processes, and cover suffosion sinkholes that have formed in the gypsum karst of Lesina Marina area, dangerously affecting the residential area during the last two decades (e.g. Fidelibus et al. 2011). The presence of the sinkholes and of the karst reactivation led to the demand of a monitoring system, for the detection of vertical displacements over a large area. To this end, SAR data acquired by the European ERS and ENVISAT satellites, spanning more than 10 years, were processed through persistent scatterer interferometry (PSI) techniques (Ferretti et al. 2001; Bovenga et al. 2004). These allow investigating millimetric displacements of the Earth surface occurring over long timespans, thanks to the regular revisit times and the uniform acquisition geometry of the used remote sensing satellites. Complete time series of displacement measurements can be derived over particular objects on the Earth surface, exhibiting radar backscattering signatures which stay coherent over time.

The analysis was initially aimed at investigating the possible evidence of subtle movements connected to the known sinkholes in the area. In fact, applications of InSAR and/or PSI to sinkhole movement monitoring has been attempted in some instances, with success (Vaccari et al. 2013; Rucker et al. 2013; Gutiérrez et al. 2011; Carbonel et al. 2014).

The most striking results of the processing showed instead the presence of steadily uplifting PS objects over the Lesina Marina urban area, in a rather smooth spatial

pattern, with maximum values located along the Acquarotta canal, with average uplift velocities reaching about 4 mm/year, and decreasing gradually towards W–SW to about zero. The peculiar nature of this pattern, with its small spatial scale, and its position on such a geologically complex and hazard-prone area, prompted us to look for a comprehensive explanation of the phenomena possibly taking place at the Lesina Marina site.

In the paper, after a description of the experimental data and methods, in “Dataset” section, we show and discuss in “Results and discussion” section the main results obtained from data processing and comparisons. Finally, in “Conclusions” section we draw some conclusions.

Geological setting

During Mesozoic, in the Adria Plate (sensu Channell et al. 1979), the narrow Adriatic pelagic basin, flanked by the two carbonate Apulian, to the SW, and Adriatic Platform, to the NE, roughly occupied the same position of the present-day Adriatic Sea (Zappaterra 1990, 1994; Bernoulli 2001), as sketched in Fig. 1a. Both the basinal and platform domains developed as a consequence of early Jurassic rifting of an epeiric area dominated by the deposition of carbonates. This carbonate platform-basin system, which developed mainly during the Mesozoic, was rooted on Norian anhydrites and shallow-water limestones and dolostones, i.e. the Burano Fm, which overlie Permian continental deposits draping the Hercynian basement (Ricchetti et al. 1988). Later, the basinal and platform domains were partially involved in the Tertiary shortening related to the Apennines and to the Dinarides–Albanides. Near and along the front of these orogens, the evaporites belonging to the Burano Fm promoted diapirism, mostly during Neogene (Underhill 1988; Zelilidis et al. 1998; Kamberis et al. 2000; Kokinou et al. 2005; Scrocca 2006; Alves et al. 2007; Geletti et al. 2008; Festa et al. 2014; Kokkalas et al. 2013).

In northern Apulia (Fig. 1a), in the Lesina Marina area, the cropping out of Triassic gypsum rocks, belonging to the Burano Fm (Fig. 1b), rose up from the deep anhydrite source (Cotecchia and Canitano 1954; Bigazzi et al. 1996). According to Bigazzi et al. (1996), hydration of anhydrites, i.e. the formation of gypsum, possibly occurred after their uprise. Up to decametric blocks of Paleocene mafic and ultramafic hypabyssal rocks (De Fino et al. 1983; Bigazzi et al. 1996) and Triassic limestones (e.g. Posenato et al. 1994), that locally crop out embedded in the gypsum rocks (e.g. Amendolagine et al. 1964), would have been dragged, from the depth, during ascent by diapirism of the gypsum body (Cotecchia and Canitano 1954) or by tectonic squeezing of the anhydrites (Bigazzi et al. 1996). As

observed in the exposed rocks by Selleri and Mastronuzzi (2003) and by Fidelibus et al. (2011), the gypsum bedrock in the subsurface of Lesina Marina, where its top gently dips toward West (Melidoro and Panaro 2000; Fidelibus et al. 2011; Caggiano et al. 2012), (Fig. 1c), shows a high density of cavities, either dissolutional conduits or voids related to gravitational collapse processes. Most of these cavities, metric in size, are partially or totally filled basically with sand deposits derived from the overlying Quaternary sedimentary cover (Melidoro and Panaro 2000). According to Selleri and Mastronuzzi (2003), these characters may be related to a probable karst undercover genesis and evolution. Recently, Fidelibus et al. (2011) have demonstrated that the changes in the hydrogeological functioning have favoured both erosion of the filling of cavities and karstification processes. Furthermore, hydrochemical evidence reveals that gypsum dissolution is a currently active process favoured by fresh water and sea water mixing and cation exchange processes; however, the dominant evolution time of gypsum dissolution is much greater than human lifetime (Campana and Fidelibus 2015).

Dataset

Satellite data and processing

We used SAR data from the European Space Agency's ERS-1/2 and ENVISAT satellites, from both ascending (24 ERS, 33 ENVISAT acquisitions) and descending geometry (32 ERS, 28 ENVISAT acquisitions), covering a total time interval from July 1992 to October 2000 (ERS), and then from September 2003 to December 2009 (ENVISAT).

The data were processed through the DORIS open source software (Kampes et al. 2003) to obtain stacks of co-registered differential interferograms, and then through the SPINUA software suite (Bovenga et al. 2004) to extract relevant information about displacements of stable points located on the area.

Tables 1 and 2 summarize data relevant to the used SAR scenes, such as the date of acquisition and the perpendicular component of the sensor baselines, i.e. the distance separating satellite orbit tracks in a plane perpendicular to the satellite trajectory from that of the reference (master) acquisition.

PSI techniques generally rely on the density of detected stable objects to extract information about spatially correlated phenomena, such as the atmospheric phase screen (APS) superimposed on the phase signal of each SAR image in a time series (Ferretti et al. 2001). When analysing scarcely urbanized areas, or, such as in this case, relatively isolated, small urban centers, it is useful to use robust approaches in extracting APS information to increase the number of detected PS. This is generally

possible by restricting the processed area, so that APS variations can be modeled with smooth functions such as low-order polynomial surfaces. The approach has been demonstrated to give good results in several instances, e.g. in the study of small-scale phenomena such as landslides in low-urbanization settings (Bovenga et al. 2006). Here, we applied the same approach to increase the number of detected PS on the urban center of Lesina Marina, which has a size of about $1 \text{ km} \times 1 \text{ km}$.

To reduce the chance of processing artefacts such as spurious velocity gradients and/or offset velocity differences, the local results were compared to global, full-frame results obtained through the same or analogous software, and to GPS data from permanent stations distributed throughout the area. The comparison, not shown here for brevity, does not show significant artefacts, thus confirming the reliability of the measurements described below.

Leveling

High-precision leveling measurements were performed on several tens of topographic points on the study area, during two ground truth campaigns, in 2000 and in 2010. The leveling measurement positions can be seen in the map in Fig. 1d, as well as on the enlarged detail map in Fig. 5. The leveling stations are located mainly close to the canal, in a strip roughly oriented in a N–S direction, about 150 m wide. All leveling measurements are expressed with respect to a given reference, corresponding to the area of the “Madalena” Hotel, shown as a magenta star in Fig. 1d.

Field and petrographic observations

Field geological mapping, sampling and petrographic observations were carried out in the Lesina Marina area. Since the Quaternary sandy deposits are very poorly exposed, although their presence is well constrained by many holes drilled in the area (Melidoro and Panaro 2000; Fidelibus et al. 2011), the geological mapping focused on Upper Triassic gypsum rocks, well exposed especially along the northern part of the Acquarotta canal (Fig. 1c). Here, the gypsum rocks appear from mainly coarse grained massive to locally finer grained layered. Within the massive portion, an intergranular lutite is often present between the larger gypsum crystals, which are euhedral to subhedral. The individual grains, that typically are colourless, vitreous and characterized by clear cleavage planes, reach a maximum size of 2–3 cm (Fig. 2a); however, white gypsum is locally present as well (Fig. 2b). Centimetric to metric in size clasts of both Paleocene mafic to ultramafic hypabissal rocks and Triassic limestones, as well as of finer grained layered gypsum rocks, locally crop out embedded in the massive gypsum matrix (Fig. 2b–d, respectively). In

Table 1 ERS dataset

Ascending				Descending			
ID	Sensor	Date	B_{\perp} (m)	ID	Sensor	Date	B_{\perp} (m)
1	E1	24/06/1995	24.7	1	E1	10/07/1992	88.0
2	E1	11/11/1995	133.3	2	E2	14/08/1992	−462.2
3	E2	12/11/1995	453.4	3	E2	23/10/1992	43.1
4	E1	16/12/1995	−911.6	4	E2	21/05/1993	95.2
5	E2	31/03/1996	−258.3	5	E1	30/07/1993	474.2
6	E2	18/08/1996	826.6	6	E1	08/10/1993	182.3
7	E2	27/10/1996	−721.6	7	E1	12/11/1993	218.7
8	E2	05/01/1997	−277.3	8	E2	24/07/1995	384.7
9	E2	16/03/1997	0.0	9	E1	02/06/1996	−231.4
10	E2	25/05/1997	−292.6	10	E2	03/06/1996	−298.7
11	E2	03/08/1997	−38.8	11	E2	12/08/1996	185.9
12	E2	01/03/1998	199.9	12	E2	16/09/1996	191.9
13	E2	10/05/1998	−235.7	13	E2	30/12/1996	255.3
14	E2	19/07/1998	−260.4	14	E2	23/06/1997	190.6
15	E2	27/09/1998	−482.6	15	E2	28/07/1997	310.1
16	E2	06/12/1998	−650.1	16	E2	10/11/1997	−73.3
17	E2	25/04/1999	108.6	17	E2	15/12/1997	−125.0
18	E2	04/07/1999	608.3	18	E2	19/01/1998	−104.9
19	E1	11/09/1999	−347.2	19	E2	23/02/1998	−204.3
20	E2	12/09/1999	−120.3	20	E2	30/03/1998	208.0
21	E2	21/11/1999	302.1	21	E2	13/07/1998	−287.0
22	E2	30/01/2000	−51.9	22	E2	17/08/1998	0.0
23	E2	09/04/2000	283.2	23	E2	21/09/1998	87.4
24	E2	18/06/2000	−1029.7	24	E2	30/11/1998	87.3
				25	E2	24/05/1999	434.0
				26	E2	02/08/1999	372.8
				27	E2	06/09/1999	−221.5
				28	E2	11/10/1999	−294.9
				29	E2	15/11/1999	473.6
				30	E2	20/12/1999	230.0
				31	E2	17/07/2000	−229.3
				32	E2	30/10/2000	424.3

addition, a layering in the gypsum massive portion is sometimes highlighted by some centimeters-thick layers of black shales (Fig. 2e). Observations of thin sections, under optical microscope in polarized transmitted light, reveal for all the samples (Fig. 2c) that gypsum crystals, usually characterized by low birefringence with first-order grey interference colours are represented by poikilocrystals with small inclusions of anhydrite, typically showing bright, second-order interference colours (Fig. 2f). It is worth to note that very fine anhydrite crystals can be also found as inclusions in the finer grained gypsum rocks. Therefore, these relationships between gypsum and anhydrite indicate that gypsum is secondary and that it formed at the expense of the original anhydrite crystals by hydration processes. In finer grained gypsum rocks the layering is well developed

and characterized by an alternation of whitish to dark greyish millimeter- to centimeter-thick layers that exhibit a plane parallel geometry (Fig. 2g); sometimes a chaotic convolute geometry is shown by this layers (Fig. 2h). Finally, a network of centimeter-thick fractures filled by secondary gypsum (Fig. 2j) crosscuts both the massive and the layered gypsum portions.

Results and discussion

For all the processed SAR data stacks, we observe a good number of PS objects quite uniformly distributed over the village area, with a few more scattered PS in the outskirts. PS displacement are measured along the satellite line of

Table 2 ENVISAT dataset

Ascending			Descending		
ID	Date	B_{\perp} (m)	ID	Date	B_{\perp} (m)
1	21/09/2003	33.5	1	04/10/2004	−107.3
2	26/10/2003	478.1	2	13/12/2004	−122.4
3	14/03/2004	−361.8	3	21/02/2005	−522.2
4	27/06/2004	371.0	4	02/05/2005	534.1
5	01/08/2004	−41.5	5	11/07/2005	774.8
6	10/10/2004	−1121.3	6	19/09/2005	−93.1
7	19/12/2004	688.7	7	28/11/2005	−159.6
8	23/01/2005	−553.9	8	06/02/2006	−646.1
9	27/02/2005	514.9	9	13/03/2006	86.1
10	08/05/2005	−777.6	10	17/04/2006	−150.8
11	17/07/2005	−489.4	11	26/06/2006	432.3
12	21/08/2005	450.3	12	04/09/2006	437.9
13	25/09/2005	−735.4	13	22/01/2007	718.0
14	04/12/2005	769.7	14	26/02/2007	70.9
15	12/02/2006	302.5	15	02/04/2007	516.0
16	23/04/2006	−711.2	16	11/06/2007	−137.2
17	02/07/2006	−821.9	17	20/08/2007	52.6
18	19/11/2006	510.1	18	29/10/2007	0.0
19	28/01/2007	−443.7	19	07/01/2008	−400.9
20	17/06/2007	0.0	20	17/03/2008	−111.9
21	26/08/2007	209.4	21	26/05/2008	−54.7
22	04/11/2007	−17.6	22	04/08/2008	112.3
23	13/01/2008	71.5	23	22/12/2008	−284.8
24	23/03/2008	162.3	24	02/03/2009	256.6
25	01/06/2008	−84.5	25	06/04/2009	577.8
26	10/08/2008	92.7	26	11/05/2009	−54.4
27	08/03/2009	−2.6	27	28/09/2009	662.1
28	28/12/2008	−86.3	28	07/12/2009	308.9
29	19/10/2008	−29.1			
30	26/07/2009	70.6			
31	17/05/2009	−112.8			
32	04/10/2009	−385.7			
33	13/12/2009	−441.8			

sight (LOS), i.e. the sensor looking direction, which is determined by the nominal incidence angle, of about 23 degrees with respect to the vertical for all the images, and the orbit heading angle with respect to the N direction, which is about 8 and 172 degrees for ascending and descending geometries, respectively. The displacement LOS mean velocities, estimated over the ERS and ENVISAT observation periods, appear spatially homogeneous, gently decreasing from positive (uplift) to slightly negative (subsidence) values in a roughly WSW direction, with a few scattered points at the west of the urban area subsiding up to -7 mm/year. The PS mean velocity maps for the four processed data stacks are shown in Fig 3a–d.

The described velocity spatial trend is present in the PS maps derived from both ascending and descending geometries, in ERS and ENVISAT data. In view of the above-mentioned controls, which allow to exclude processing artefacts, the presence of such a steady uplift signal in both time series periods appears striking, and claims for a geophysical interpretation.

Relying on the relatively smooth nature of the observed phenomenon, average velocities from ascending and descending PS data were interpolated through Kriging (Isaaks and Srivastava 1989) over a common geographic grid, with 30 m posting, then combined to obtain vertical (up-down) and east–west velocity components, denoted by $\langle v_U \rangle$ and $\langle v_E \rangle$, according to the following equations:

$$\langle v_U \rangle = \frac{\langle v_A \rangle + \langle v_D \rangle}{2 \cos \theta}; \langle v_E \rangle = \frac{\langle v_A \rangle - \langle v_D \rangle}{2 \sin \theta}, \quad (1)$$

where $\langle v_A \rangle$ and $\langle v_D \rangle$ are the ascending and descending interpolated mean velocity fields, respectively, and θ is the SAR sensor look angle. The third, north–south component of movement is hardly retrievable from satellite InSAR data, due to the geometric configuration of the spacecraft orbit, which causes the LOS to have very small north–south projection (e.g. Samiei-Esfahany et al. 2010). In our case, north–south motion can be assumed negligible, due to the geographic configuration of the test site, with the Acquarotta canal running roughly in a N–S direction. Therefore, this component of displacements is ignored in the following.

Derived vertical displacement rates for ERS data (see Fig. 3e) reach ~ 4 mm/year on locations adjacent to the canal, gently decreasing to slightly negative values towards the western end of the built-up area (about 600 m away). Similar values are derived from ENVISAT data (Fig. 3f), with somewhat lower maximum values on the canal, and a slightly more pronounced decrease towards the West. The east–west velocity component for the ERS data (Fig. 3g) also show a W–SW trend, with rates going from about zero close to the canal, to about -1 to -2 mm/year (i.e. towards the West), on the westwards margin of the town area. Slightly lower values are reached in the ENVISAT data (Fig. 3g).

Comparison with leveling data

Mean displacement velocities derived from each leveling data point were compared with the nearest PSI measurements within a fixed search radius of 50 m. Mean ascending and descending PSI velocities within this search radius were combined to derive the vertical and horizontal motion components, as in (1). The $\langle v_U \rangle$ values derived in this way were then compared to the leveling measurements. Plots of the two data series are shown in Fig. 4, as a

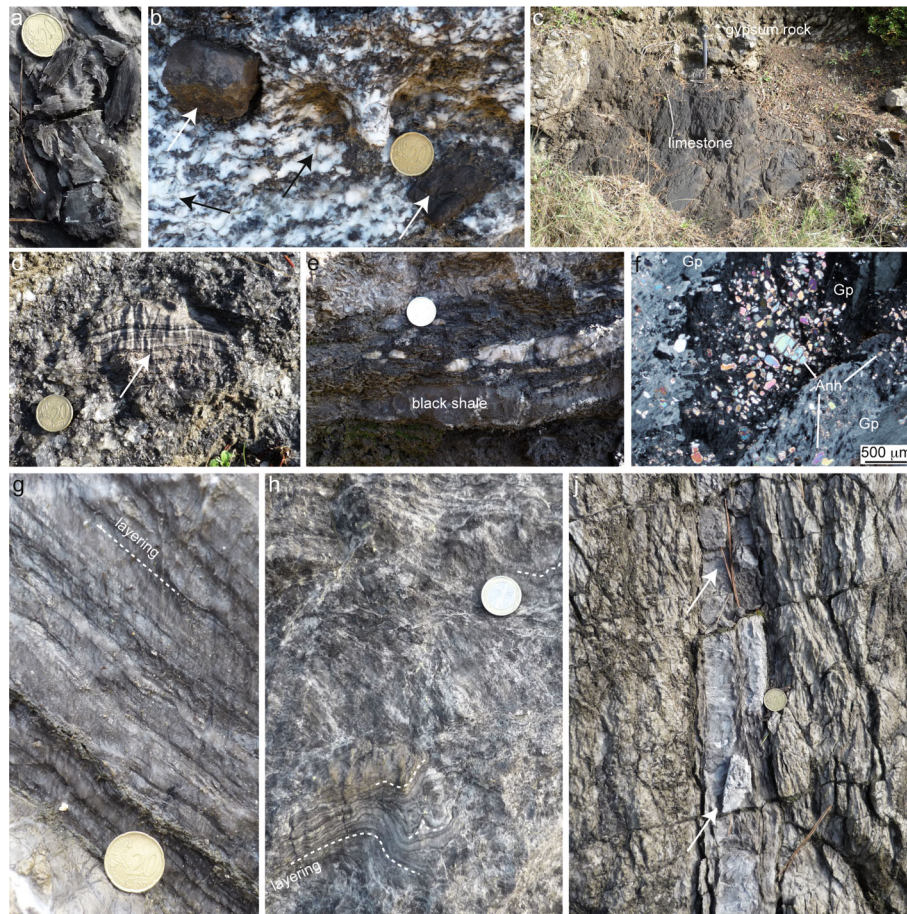


Fig. 2 **a** Colourless and vitreous large crystals of gypsum. The cleavage planes can be also appreciated. **b** Centimetric clasts of Paleocene ultramafic rocks (*white arrows*) within the massive gypsum matrix, in which *white* gypsum crystals (*black arrows*) can be appreciated. **c** Metric block of Triassic limestone within the massive gypsum rocks. **d** Decimetric finer grained layered gypsum fragmented (*white arrow*) within the massive gypsum matrix. **e** Centimeter-thick layer of *black shale* within the massive gypsum

rocks. **f** Thin section micrograph (crossed polars) showing gypsum (Gp) poikilocrystals with inclusions of anhydrite (Anh; mineral abbreviations after Kretz 1983). **g** Whitish to dark greyish millimeter- to centimeter-thick layers with plane parallel geometry in finer grained gypsum rocks. **h** Convolute layers in finer grained gypsum rocks. **j** Fractures filled by secondary gypsum (*white arrows*) crosscutting massive gypsum rocks

function of the northings UTM coordinate. In the figure, PS velocities' error bars are derived from estimates of the phase dispersion (Bovenga et al. 2006). Uncertainties on leveling mean velocities can only be inferred from nominal accuracy values of each of the two measurements, and are negligible compared to the former. As can be seen, apart from a vertical offset due to the different chosen reference point, the two trends look similar. Differences are contained within ± 2 mm/year, with a mean error of about 1.5 mm/year and a standard deviation of about 0.54 mm/year. The correlation between the two measurements is about 0.62, thus the hypothesis that PS vertical velocity is statistically independent of leveling velocity can be ruled out with a high level of confidence (>99 % using Fisher's test).

These figures seem in agreement with those reported in several comparisons of PS-derived velocity measurements

with ground-based leveling, see e.g. Perissin et al. (2007), or Crosetto et al. (2007). A few examples of time series of PS points close to leveling stations, including one possibly corresponding to a sinkhole collapse site, are reported in the following sections. This validation of the ENVISAT data allows to safely confirm also the trends observed from the ERS data, which show basically similar characteristics, thus depicting a regional uplift phenomenon going on in a rather steady way over the total ~ 17 -year timespan of SAR observations.

PS time series

Figure 5 shows sample time series of PS close to leveling stations, represented as coloured triangles, with colour coded according to the measured average displacement rates.

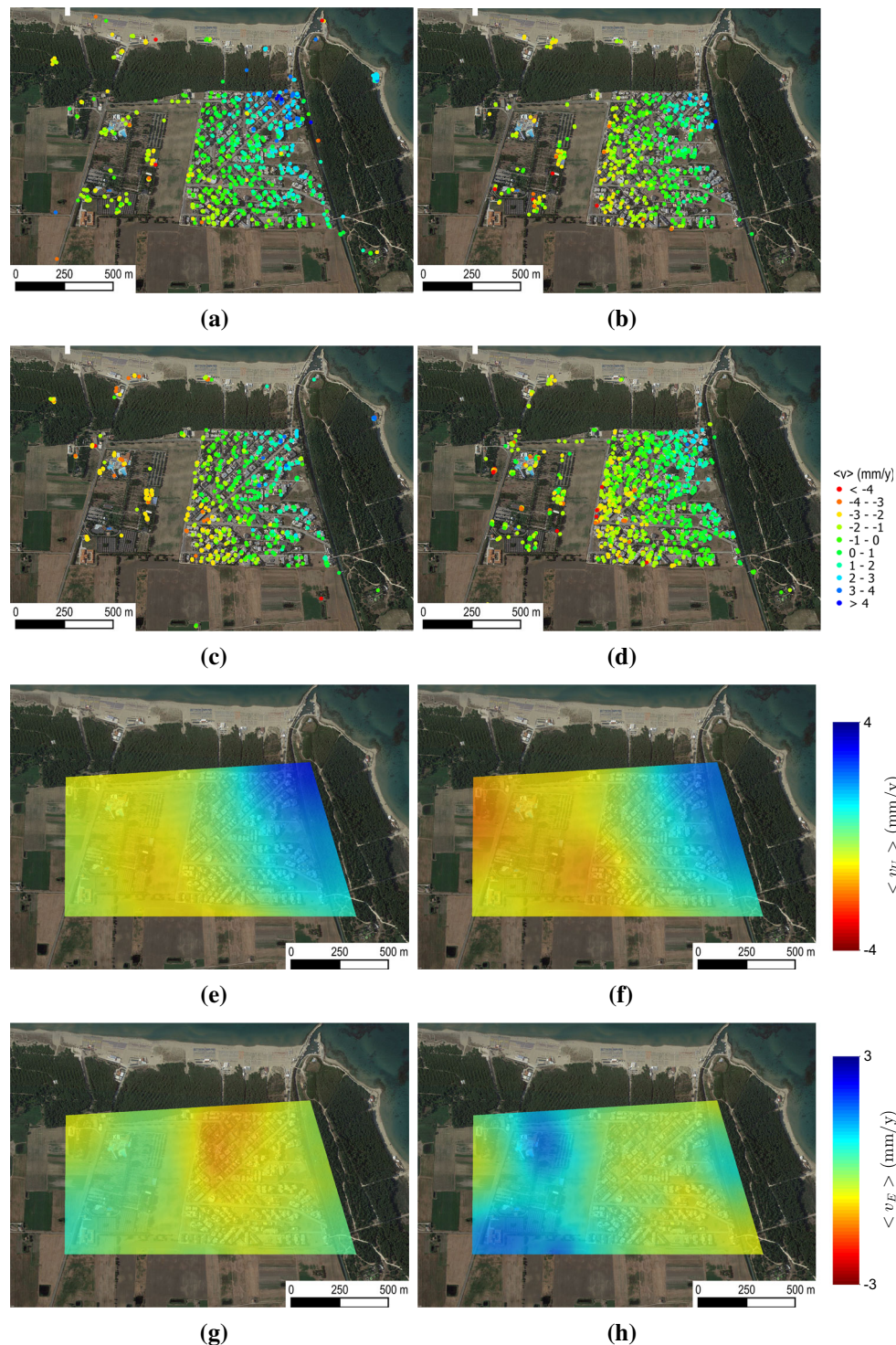


Fig. 3 Top panels PSI mean velocity maps from ERS ascending (a), ERS descending (b), ENVISAT ascending (c) and ENVISAT descending (d) geometry. Bottom panels up-down (e-f) and east-

west (g-h) component of the velocity from the ERS (e-g) and ENVISAT (f-h) time series. Interpolation is restricted to the area with good PS density

On the right of Fig. 5 we show plots of sample deformation time series of clusters of PS, together with the displacement history of nearby leveling points, i.e. their positions as measured in the two leveling campaigns. PS points are selected in this case as those lying on positions

likely belonging to the same building, as can be deduced by the map on the left.

PS displacements are defined relative to the position in the master acquisition; the leveling deformation lines were also shifted vertically so as to refer them to the master

Fig. 4 Northings profile of the vertical velocity measurements from leveling (*blue circles*) and PS (*red squares*, with error band). The *star* indicates the reference point of the leveling data

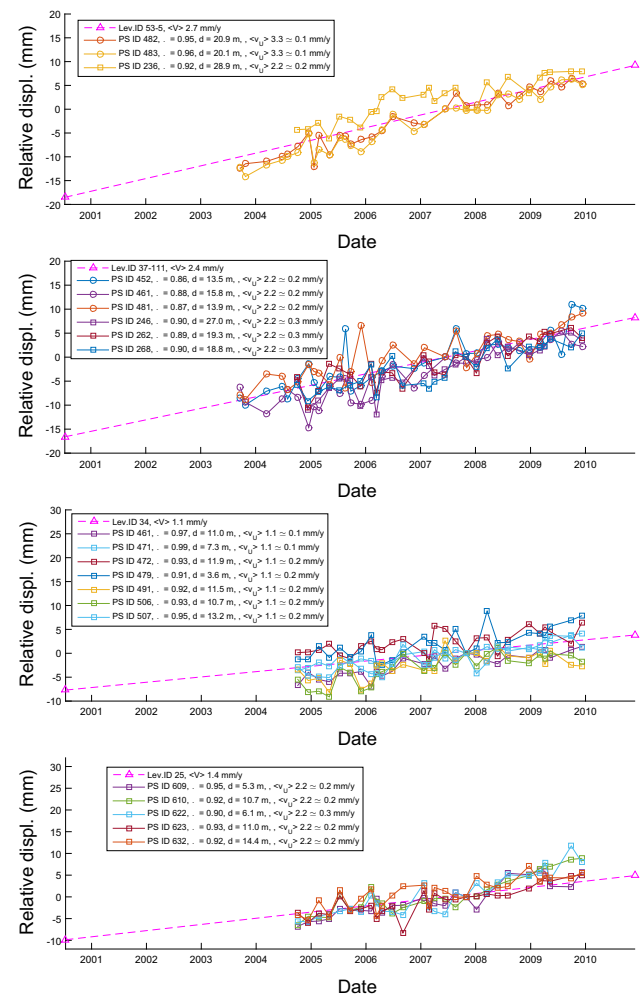
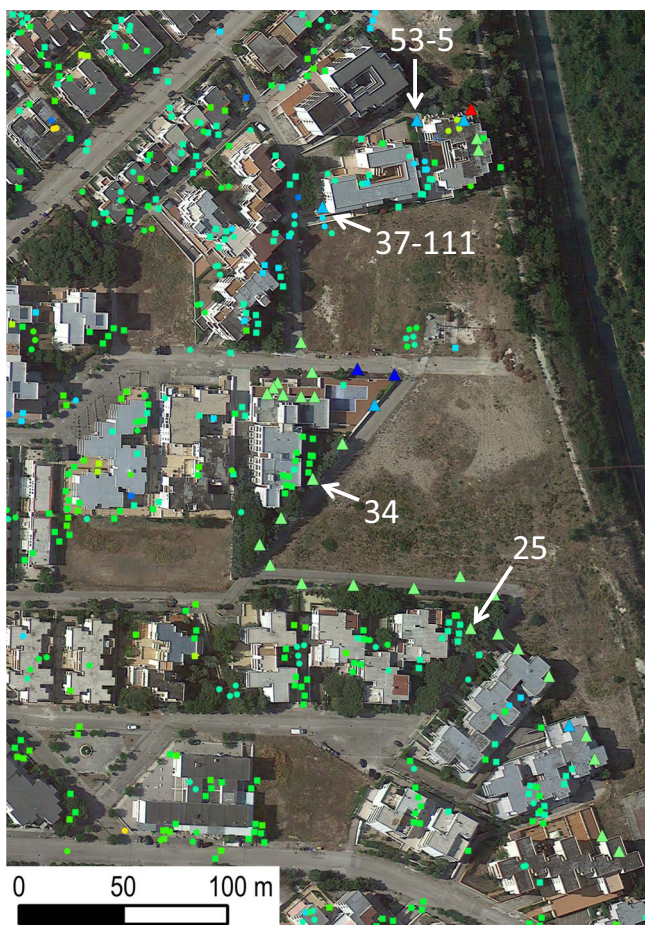
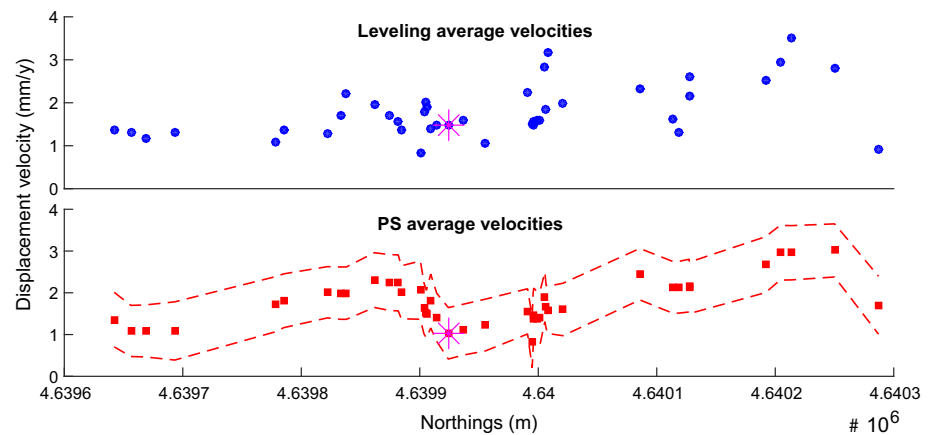


Fig. 5 Left PS velocity and leveling measurements map. Colour scales are the same as in Figs. 3 and 6, respectively. Right displacement time series of four sample leveling stations, indicated by the labels on the left, and the closest PS points. PS data are vertical

acquisition date. Therefore, the position of the vertical axis origin in the three plots is to be considered arbitrary. Also, leveling displacement rates are corrected for the offset

velocity components, computed in the hypothesis of null horizontal movement. Both PS and leveling time series are referred to the respective master SAR image date, so that in all the three plots the vertical scale origin is arbitrary

value calculated on the reference Maddalena Hotel point, i.e. 1.48 mm/year. As the sample points are located close to the canal path, where no significant lateral displacements

are observed (see Fig. 3) we convert LOS-projected PS individual velocities to vertical velocities by assuming a null horizontal velocity component, then using the transformation $v_U = v_{A/D} / \cos \theta$, as can be deduced by (1) by assuming $v_E = 0$.

As can be seen, in all cases the agreement of the PS time series with the leveling displacements looks satisfactory. The oscillations in the PS time series displacements, enhanced by the small scale of the plots' y-axis, are due in part to the absence of any filtering in the temporal dimension. Apart from this, no significant departures from a linear displacement behaviour are visible for all the points.

Local analysis

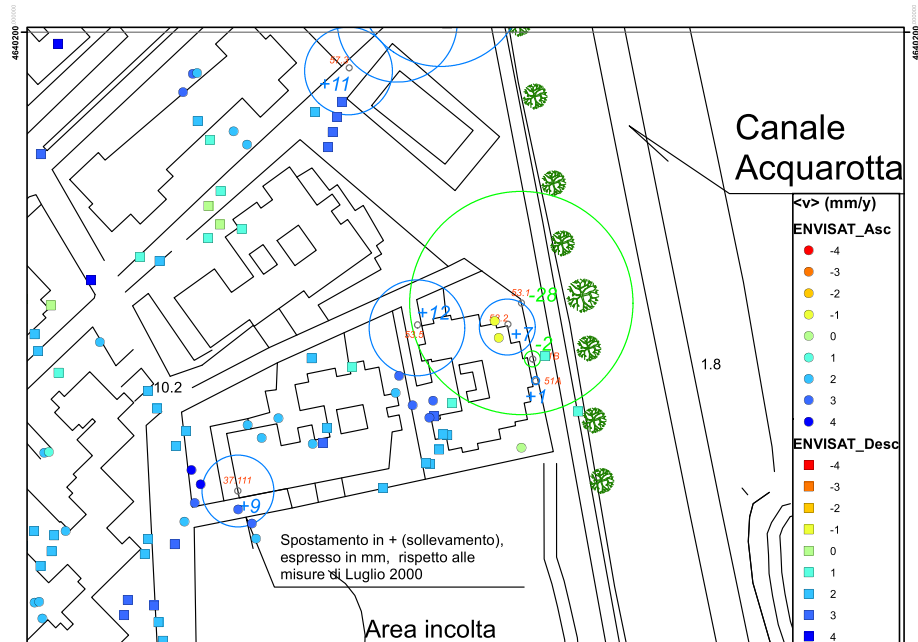
In Fig. 6 we show a zoom map around a pair of detected PS close to a single leveling measurements which reported a decreasing height of up to 28 mm in 10 years. The PS points closest to these subsiding leveling benchmarks exhibit a slow downward movement, of about -1 mm/year. Compared to the surrounding, positive uplift velocity values, around $2-3$ mm/year, this means a relative subsidence (negative) rate of about $3-4$ mm/year.

Displacement time series of the mentioned two PS, as well as a relative mean displacement of the nearby leveling benchmark, are shown in Fig. 7. The time series seem to indicate a relatively fast subsidence during the years 2005 and 2006, followed by a relatively more stable behaviour. This seems compatible with the total displacement measured by the leveling.

Due to the known widespread presence of several sinkholes in the Lesina Marina area, it is tempting to associate these localized, isolated displacement time series with the precursory movements associated with a nearby, possibly undetected sinkhole. However, no other clear instances of moving PS close to sinkholes could be reliably determined on the site. The most likely explanation is that in the period between 1999 and 2008, the distribution of newly detected sinkholes reveals a trend towards a clustering with old ones, rather than a random positioning (see e.g. fig. 8 in Caporale et al. 2013). This is in line with the general rock mass behaviour, as gathered by numerous direct and geophysical surveys carried out, in terms of rock fracturing and subsequent anisotropy of permeability (Spilotro et al. 2009), and the resulting groundwater flow (Campana and Fidelibus 2015). As a consequence, areas affected by sinkholes in the period covered by the SAR data were left free of man-made urban structures, and are therefore lacking PS. The only exception is the above-mentioned single cluster of PS, belonging, as described, to a building sufficiently close to anomalous measurements of the leveling data, which however lack direct evidence of nearby sinkholes.

In fact, sinkholes usually develop on small timescales, over limited spatial areas, and are therefore considered at the limit of applicability of spaceborne remote sensing techniques. Some recent examples of applications of SAR interferometry to sinkhole detection and/or monitoring can be found, e.g. in Bruno et al. (2008), or Gutiérrez et al. (2011). It is usually argued that sinkhole phenomena occur suddenly in landscapes characterized by rocks or other

Fig. 6 ENVISAT ascending (coloured circles) and descending (coloured squares) PS, over a cadastral map of the area in the vicinity of a detected sinkhole. Larger circles in green are centered on points where leveling detected subsidence (circle radius proportional to subsidence rate)



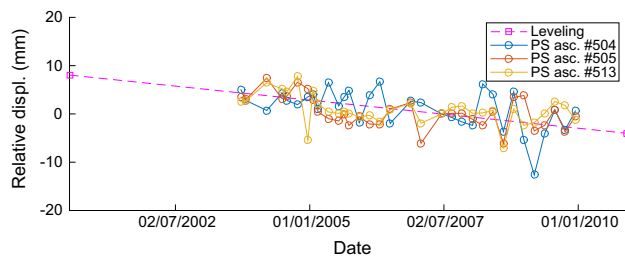


Fig. 7 Time series of the two ENVISAT Ascending PS points close to the sinkhole. The *dashed line* shows the relative displacement recorded by the nearest leveling benchmark shown in Fig. 6

kinds of substrate with limited deformation capabilities. Nevertheless, the chance of detecting small precursory terrain movements in correspondence to sinkholes can be increased, when the sinkhole phenomenon occurs on a site with a cover of sand, clay or other compactable material. In such cases, in fact, small precursory episodic deformations, per se not detectable by remote sensing, could cause stronger compaction phenomena in the soft cover, which could be detected as small movements preceding the final catastrophic collapse.

A geological Interpretation

From a geological point of view, these results are not of immediate interpretation. The investigated area affected by the uplift (Ciaranfi et al. 1983; Mastronuzzi and Sansò 2002) coincides with the higher part of a salt dome (Cotecchia and Canitano 1954). Therefore, according to the conclusions made by Festa et al. (2014) about the near Tremiti diapir (Fig. 1b), a still active diapirism cannot be excluded also for the diapir of the Lesina Marina area. An uplift rate of ca. 1 mm/year can be estimated for the Tremiti diapir, since, according to Festa et al. (2014), a distance upwards of ca. 5000 m was covered by this diapir in the last ca. 5 Ma. This uplift rate shows some correlation with that inferred by Mastronuzzi and Sansò (2002) for the Holocene, nearby Lesina Marina, i.e. 1.5 mm/year.

However, our data point to uplift rates well above that value, i.e. up to about 4 mm/year. Accordingly, a further contribution to uplift, in addition to that due to diapirism, may be related to the transformation of anhydrite in gypsum (Fig. 2f). As demonstrated in several studies (Pettijohn 1957; Bell et al. 1986; Azam 2006; Rauh and Thuro 2007), this transformation involves a volume increase of up to ca. 60 % of the hydrating mass. Therefore, the hydration of the residual anhydrite surface could have determined, and could continue to determine, a volume increase of the gypsum mass in the area of Lesina Marina. This phenomenon may have been accelerated by an increase in circulation of the water in the fractured bedrock due to the Acquarotta canal, along which the maximum uplift rates

have been recorded, especially in its northern part (Fig. 3e, f). Here, the horizontal movements are practically absent, whereas they have been recorded, together with the subsidence, at the western side of the area with maximum uplift rates (Fig. 3g, h), as would be expected. More quantitative evaluations or modeling about the volumetric expansion of the sulphate rock mass would have to rely on at least the amount of anhydrite/gypsum transformation, as well as on the geometrical 3D reconstruction of the sulphate rock body. Unfortunately, these quantitative evaluations would be highly speculative due to both the high heterogeneity of these sulphate rocks (i.e. random variations of volume percentages of anhydrite and gypsum) and the not currently available deep data. In this respect, as a final remark, it is worth noting that the anhydrite/gypsum transformation has been observed to cause consistent and sudden uplift phenomena on other sites, such as the city of Staufen, Germany (Lubitz et al. 2014), causing serious infrastructure damages.

Conclusions

We show results of the monitoring of the Lesina Marina area in Southern Italy, a tourist village plagued by the formation of sinkholes in the vicinity of an artificial canal cutting the area since the thirties. ERS and ENVISAT ascending and descending SAR data, processed through PSI techniques, show displacement velocities degrading spatially from a maximum, positive value in a strip close to the canal, towards null values at the western part of the urban area, with a few scattered subsiding points. High-precision leveling, performed in two ground campaigns in 2000 and 2010, was compared to the PS-derived vertical velocity maps from ENVISAT data.

Comparison between leveling mean velocities and PS mean vertical velocities reveals a good overall agreement, compatible with current state of the art PSI accuracy assessments. The velocity differences exhibit a small-dispersion distribution of the residuals, apart from a bias due to the different reference points in the two techniques. The similarity of the ERS data series thus points to a steady uplift phenomenon covering the entire ~17-year timespan of SAR observations. The available dataset has been tentatively interpreted as the result of anhydrite/gypsum transformation that is still provoking a volume increase of the hydrated gypsum mass and, accordingly, uplift rates well above those attributable to the solely diapiric phenomenon.

It should be noticed that the available leveling stations are located mostly close to the canal path, disposed in a roughly N–S direction, thus perpendicular to the direction of main variation of the uplift phenomenon. Further

measurements along this latter direction would probably add information to this study. Moreover, recent and higher resolution SAR data will likely help in shedding light on the actual processes taking place in this interesting site.

The petrographic observations cannot alone reveal if the anhydrite/gypsum transformation is still active. As demonstrated in the present case study, SAR interferometry and in situ measurements may represent an essential tool to infer if the hydration of anhydrite is under development. Therefore, the integration between both petrographic and geophysical investigations should be used to influence the engineering design choices for the risk mitigation in those urbanized areas characterized by the presence of sulphate rocks.

Acknowledgments Research funded through the Italian Ministry of Research—PRIN 2008 research grant “Advanced technologies in the assessment and mitigation of the landslide risk: precursors detection, previsional models and thematic mapping”. ENVISAT and ERS data are copyright of European Space Agency—provided under Category-1 project N. 5367, “Subsidence monitoring in Daunia and Capitanata (Puglia Region, Italy) through multi-temporal point-target DInSAR techniques”. GAP srl personnel is acknowledged for aid in InSAR processing.

Open Access This article is distributed under the terms of the Creative Commons Attribution 4.0 International License (<http://creativecommons.org/licenses/by/4.0/>), which permits unrestricted use, distribution, and reproduction in any medium, provided you give appropriate credit to the original author(s) and the source, provide a link to the Creative Commons license, and indicate if changes were made.

References

- Alves TM, Lykousis V, Sakellariou D, Alexandri S, Nomikou P (2007) Constraining the origin and evolution of confined turbidite systems: southern Cretan margin, Eastern Mediterranean Sea (34°30–36°N). *Geo-Mar Lett* 27(1):41–61. doi:10.1007/s00367-006-0051-1
- Amendolagine M, Dell’Anna L, Ventriglia U (1964) Alcune rocce ignee alla Punta delle Pietre Nere presso Lesina (Provincia Foggia). *Periodico di Mineralogia* 33:337–444 (in Italian)
- Azam S (2006) Study on the geological and engineering aspects of anhydrite/gypsum transition in the Arabian Gulf coastal deposits. *Bull Eng Geol Environ* 66(2):177–185. doi:10.1007/s10064-006-0053-2
- Bell F, Cripps J, Culshaw M (1986) A review of the engineering behaviour of soils and rocks with respect to groundwater. *Geol Soc Lond Eng Geol Spec Publ* 3:1–23. doi:10.1144/GSL.ENG.1986.003.01.01
- Bernoulli D (2001) Mesozoic-tertiary carbonate platforms, slopes and basins of the external apennines and sicily. In: Vai G, Martini I (eds) *Anatomy of an Orogen: the Apennines and Adjacent Mediterranean Basins*. Springer Netherlands, pp 307–325. doi:10.1007/978-94-015-9829-3_18
- Bigazzi G, Laurenzi M, Principe C, Brocchini D (1996) New geochronological data on igneous rocks and evaporites of the Pietre Nere Point (Gargano peninsula, southern Italy). *Boll Soc Geol Italy* 115:439–448
- Boni A, Casnedi R, Centamore E, Colantoni P, Cremonini G, Elmi C, Moneto A, Selli R, Valletta M (1969) Note illustrative alla Carta Geologica d’Italia, F. 155 San Severo. Servizio Geologico d’Italia, Roma (in Italian)
- Bovenga F, Refice A, Nutricato R, Guerriero L, Chiaradia MT (2004) SPINUA: a flexible processing chain for ERS/ENVISAT long term interferometry. In: *Proceedings of the 2004 Envisat & ERS symposium*, Salzburg, Austria, ESA SP-572 (CD-ROM)
- Bovenga F, Nutricato R, Refice A, Wasowski J (2006) Application of multitemporal differential interferometry analysis for detecting slope instability in urban/peri-urban areas. *Eng Geol* 88:218–239. doi:10.1016/j.enggeo.2006.09.015
- Bruno E, Calcaterra D, Parise M (2008) Development and morphometry of sinkholes in coastal plains of Apulia, southern Italy. Preliminary sinkhole susceptibility assessment. *Eng Geol* 99(3–4):198–209. doi:10.1016/j.enggeo.2007.11.017
- Caggiano T, Denora D, Garofalo G, Versace P, Di Santo A (2012) Zonazione della pericolosità dell’abitato di Lesina Marina—FG. In: *Atti del XXXIII Convegno Nazionale di Idraulica e Costruzioni Idrauliche*, Brescia (in Italian)
- Campana C, Fidelibus MD (2015) Reactive-transport modelling of gypsum dissolution in a coastal karst aquifer in Puglia, southern Italy. *Hydrogeol J* 23(7):1381–1398. doi:10.1007/s10040-015-1290-x
- Caporale F, De Venuto G, Leandro G, Spilotro G (2013) Interventi di mitigazione del rischio da sinkholes nell’area di Lesina marina (Provincia di Foggia, Italia). *Memorie Descrittive della Carta Geologica d’Italia XCIII*:121–141 (in Italian)
- Carbonel D, Rodríguez-Tribaldos V, Gutiérrez F, Galve JP, Guerrero J, Zarroca M, Roqué C, Linares R, McCalpin JP, Acosta E (2014) Investigating a damaging buried sinkhole cluster in an urban area (Zaragoza city, NE Spain) integrating multiple techniques: geomorphological surveys, DInSAR, DEMs, GPR, ERT, and trenching. *Geomorphology*. doi:10.1016/j.geomorph.2014.02.007
- Carella R (1963) Eruttivi di S. Giovanni in Pane e della Punta delle Pietre Nere (Gargano). *Bollettino della Società Geologica Italiana* 82(1):97–109 (in Italian)
- Channell J, d’Argenio B, Horvath F (1979) Adria, the African promontory. *Mesozoic Mediterranean palaeogeography*. *Earth Sci Rev* 15(3):213–292. doi:10.1016/0012-8252(79)90083-7
- Ciaranfi N, Ghisetti F, Guida M, Iaccarino G, Lambiasi S, Pieri P, Rapisardi L, Ricchetti G, Torre M, Tortorici L, Vezzani L (1983) Carta neotettonica dell’Italia meridionale. *Pubbl. n. 515 del Prog. Final. Geodin., CNR* (in Italian)
- Cotecchia V, Canitano A (1954) Sull’affioramento delle Pietre Nere al Lago di Lesina. *Boll Soc Geol Italy* 73:1–16 (in Italian)
- Cremonini G, Elmi C, Selli R (1971) Note illustrative della Carta Geologica d’Italia, scala 1:100.000, Foglio 156 S. Marco in Lamis. Servizio Geologico d’Italia, Roma (in Italian)
- Crosetto M, Agudo M, Raucoules D, Bourguin B, de Michele M, Le Cozannet G, Bremmer C, Veldkamp JG, Tragheim D, Bateson L, Engdahl M (2007) Validation of persistent scatterers interferometry over a mining test site: results of the PSIC4 project. In: *Proceedings of Envisat symposium 2007*, ESA SP-636
- De Fino M, La Volpe L, Piccarreta G (1983) Mafic minerals from Punta delle Pietre Nere subvolcanics (Gargano, Southern Italy): Their petrological significance. *Tschermaks mineralogische und petrographische Mitteilungen* 32(1):69–78. doi:10.1007/BF01081545
- Fantoni R, Franciosi R (2010) Tectono-sedimentary setting of the Po plain and adriatic foreland. *Rendiconti Lincei* 21(1):197–209. doi:10.1007/s12210-010-0102-4
- Ferretti A, Prati C, Rocca F (2001) Permanent scatterers in SAR interferometry. *IEEE Trans Geosci Remote Sens* 39(1):8–20. doi:10.1109/36.898661

- Festa V, Teofilo G, Tropeano M, Sabato L, Spalluto L (2014) New insights on diapirism in the Adriatic Sea: the Tremiti salt structure (Apulia offshore, southeastern Italy). *Terra Nova* 26(3):169–178. doi:[10.1111/ter.12082](#)
- Fidelibus MD, Gutiérrez F, Spilotro G (2011) Human-induced hydrogeological changes and sinkholes in the coastal gypsum karst of Lesina Marina area (Foggia Province, Italy). *Eng Geol* 118:1–19. doi:[10.1016/j.enggeo.2010.12.003](#)
- Geletti R, Del Ben A, Busetti M, Ramella R, Volpi V (2008) Gas seeps linked to salt structures in the Central Adriatic Sea. *Basin Res* 20(4):473–487. doi:[10.1111/j.1365-2117.2008.00373.x](#)
- Gutiérrez F, Galve JP, Lucha P, Castañeda C, Bonachea J, Guerrero J (2011) Integrating geomorphological mapping, trenching, InSAR and GPR for the identification and characterization of sinkholes: A review and application in the mantled evaporite karst of the Ebro Valley (NE Spain). *Geomorphology* 134(1–2):144–156. doi:[10.1016/j.geomorph.2011.01.018](#)
- Isaaks E, Srivastava R (1989) *Applied geostatistics*. Oxford University Press, New York
- Kamberis E, Sotiropoulos S, Aximniotou O, Tsaila-Monopoli S, Ioakim C (2000) Late Cenozoic deformation of the Gavrovo and Ionian zones in NW Peloponnesos (Western Greece). *Ann Geophys*. doi:[10.4401/ag-3679](#)
- Kampes B, Hanssen R, Perski Z (2003) Radar interferometry with public domain tools. In: *Proceedings of the FRINGE 2003, ESA-ESRIN, Frascati, Italy (CD-ROM)*
- Kokinou E, Kamberis E, Vafidis A, Monopolis D, Ananiadis G, Zelilidis A (2005) Deep seismic reflection data from offshore western Greece: a new crustal model for the ionian sea. *J Pet Geol* 28(2):185–202. doi:[10.1111/j.1747-5457.2005.tb00079.x](#)
- Kokkalas S, Kamberis E, Xypolias P, Sotiropoulos S, Koukouvelas I (2013) Coexistence of thin- and thick-skinned tectonics in zakynthos area (Western Greece): insights from seismic sections and regional seismicity. *Tectonophysics* 597–598:73–84. doi:[10.1016/j.tecto.2012.08.004](#)
- Kretz R (1983) Symbols for rock-forming minerals. *Am Mineral* 68(1–2):277–279
- Lubitz C, Motagh M, Kaufmann H (2014) Ground surface response to geothermal drilling and the following counteractions in Staufen im Breisgau (Germany) investigated by TerraSAR-X time series analysis and geophysical modeling. *Remote Sens* 6:10571–10592. doi:[10.3390/rs61110571](#)
- Martinis B, Pieri M (1964) Alcune notizie sulla formazione evaporitica del Triassico superiore nell'Italia centrale e meridionale. *Mem Soc Geol Italy* 4:649–678 (in Italian)
- Mastronuzzi G, Sansò P (2002) Holocene uplift rates and historical rapid sea-level changes at the Gargano promontory, Italy. *J Quat Sci* 17(5–6):593–606. doi:[10.1002/jqs.720](#)
- Melidoro G, Panaro N (2000) Sprofondamenti carsici nei gessi costieri di marina di lesina (gargano) e mitigazione del rischio. *Geologia Tecnica e Ambientale* 3:593–606 (in Italian)
- Perissin D, Prati C, Rocca F, Li D, Liao M (2007) Multi-track PS analysis in Shanghai. In: *Proceedings of the Envisat symposium 2007, ESA SP-636*
- Pettijohn F (1957) *Sedimentary rocks*, 2nd edn. Harper & Bros, New York
- Posenato E, De Fino M, La Volpe L, Piccarreta G (1994) L'affioramento del trias superiore delle pietre nere (calcarei e gessi) e i prodotti del vulcanesimo basico paleogenico. In: *Guida all'escursione generale pregressuale e alla escursione tematica sul Cretaceo murciano—77a Riunione Estiva, Congresso Nazionale della S.G.I., Geologia delle aree di avampaese*, pp 19–23 (in Italian)
- Rauh F, Thuro K (2007) Investigations on the swelling behavior of pure anhydrite. In: *Proceedings of the 1st Canada-US rock mechanics symposium—rock mechanics meeting society's challenges and demands*, pp 527–534
- Ricchetti G, Ciaranfi N, Luperto Sinni E, Mongelli F, Pieri P (1988) Geodinamica ed evoluzione sedimentaria e tettonica dell'Avampae Apulo. *Mem Soc Geol Italy* 41:57–82 (in Italian)
- Rucker M, Panda B, Meyers R, Lommler J (2013) Using InSAR to detect subsidence at brine wells, sinkhole sites, and mines. *Carbonates Evaporites* 28(1–2):141–147. doi:[10.1007/s13146-013-0134-9](#)
- Samiei-Esfahany S, Hanssen RF, Thienen-visser KV, Muntendam-bos A (2010) On the Effect of Horizontal Deformation in InSAR subsidence estimates. In: *FRINGE 2009 workshop proceedings, ESA-SP-677*
- Scrocca D (2006) Thrust front segmentation induced by differential slab retreat in the apennines (Italy). *Terra Nova* 18(2):154–161. doi:[10.1111/j.1365-3121.2006.00675.x](#)
- Selleri G, Mastronuzzi G (2003) Le aree carsiche gessose d'italia: Puglia. In: *Ist. It. Di Speleologia, Memoria* 14, 2, pp 231–240 (in Italian)
- Spilotro G, Canora F, Fidelibus MD (2009) Anisotropy of hydraulic conductivity through shallow geophysical surveys. In: *Proceedings of the international conference on rock joints and jointed rock masses, Tucson, AZ*
- Underhill JR (1988) Triassic evaporites and plio-quaternary diapirism in Western Greece. *J Geol Soc* 145(2):269–282. doi:[10.1144/gsjgs.145.2.0269](#)
- Vaccari A, Stuecheli M, Bruckno B, Hoppe E, Acton ST (2013) Detection of geophysical features in InSAR point cloud data sets using spatiotemporal models. *Int J Remote Sens* 34(22):8215–8234. doi:[10.1080/01431161.2013.833357](#)
- Zappaterra E (1990) Carbonate paleogeographic sequences of the periadriatic region. *Boll Soc Geol Italy* 109:5–20
- Zappaterra E (1994) Source-rock distribution model of the periadriatic region. *AAPG Bull* 78:333–354
- Zelilidis A, Kontopoulos N, Avramidis P, Piper D (1998) Tectonic and sedimentological evolution of the pliocene-quaternary basins of Zakynthos island, Greece: case study of the transition from compressional to extensional tectonics. *Basin Res* 10(4):393–408. doi:[10.1046/j.1365-2117.1998.00075.x](#)